INTERMETALLICS
SUBMITTED MANUSCRIPT

Crystal structure and physical properties of UMo_3B_7

L. Salamakha[1], O. Sologub[1,*], C. Rizzoli[2], H. Michor[1],
A. P. Gonçalves[3], P. Rogl[4], E. Bauer[1]

[1] *Institute of Solid State Physics, TU Wien, A-1040 Wien, Austria*

[2] *Dipartimento di Chimica, Università degli Studi di Parma, Parco Area delle Scienze 17/A, 43124 Parma, Italy*

[3] *C^2TN, Instituto Superior Técnico, Universidade de Lisboa, Estrada Nacional 10, 2695-066 Bobadela LRS, Portugal*

[4] *Institute of Materials Chemistry and Research, University of Vienna, A-1090 Vienna, Austria*

ABSTRACT

A novel ternary compound, UMo_3B_7, has been synthesized by arc melting and annealing at 900 °C. Its crystal structure was determined from X-ray single crystal diffraction data (YMo_3B_7-type structure, space group *Pnma*; *a*=1.10310(8) nm, *b*=0.30995(2) nm, *c*=1.2792(1) nm, R_F^2=0.0205). The structure is composed of boron filled trigonal prisms as well as unfilled tetrahedra and tetragonal pyramids formed by metal atoms. With respect to boron atoms aggregation, it exhibits a well-developed two-dimensional boron network revealing infinite bands of edge linked boron hexagons. The relationship with the members of the structural series within the V-B system: V_nB_{n+1}= (n-1)VB (CrB-type) + VB_2 (AlB_2-type) (n=1, 2, 3, 5) is discussed. Specific heat, magnetic susceptibility and electrical resistivity measurements characterizes UMo_3B_7 as a spin fluctuating system.

Keywords: uranium molybdenum boride; crystal chemistry; electrical resistivity; magnetic susceptibility; specific heat; X-ray diffraction.

* Corresponding author.
E-mail address: oksana.sologub@univie.ac.at (O. Sologub)

1. Introduction

Among boron rich borides, compounds with structures based on boron nets have triggered considerable scientific attention due to the important role of boron networks for distinct physical properties. Two-dimensional networks of boron atoms have been found in various structures including (i) MgB_2 with metal layers sandwiched by planar boron honeycomb layers, which were also reported to play an important role for the superconducting behaviour of this compound [1,2], (ii) heavy fermion superconductor β-$YbAlB_4$ exhibiting Yb and Al atoms located in the interlayer space of planar B_5- and B_7- rings [3-7], (iii) Y_2ReB_6-type structure where the planar nets are formed by B_5-, B_6- and B_7 rings [8], (iv) structures with puckered nets of squares, pentagons, heptagons and irregular polygons, etc. [9]. The structures of boron rich compounds of *f*-element - transition metal - boride systems are also rewarding subjects for elucidating the structural modifications and defects which play an important role for, e.g., structure stabilization of $Mg_2M_{0.75}B_{6.50}$ (M = Rh, Ir) [10, 11], or, for instance, low temperature magnetic anomalies of $TmAlB_4$ [12-14].

Earlier investigations of uranium molybdenum borides [15] defined the crystal structures of two ternary phases: $UMoB_4$ with $ThMoB_4$-type structure, space group *Cmmm* [16] and U_2MoB_6 (Y_2ReB_6-type structure, space group *Pbam*) [17]. Later on, a new $U_5Mo_{10}B_{24}$ structure (own structure type, space group *Pmmn*) which exhibits three kinds of boron polyanions - two-dimensionally infinite, puckered sheets consisting of six- and eight-membered rings; planar ribbons of condensed B_6-rings; chains of condensed B_8-rings - was discovered by Konrad and Jeitschko [18]. Although it was believed that $U_5Mo_{10}B_{24}$ corresponds to "UMo_2B_6", reported by Kuz'ma et al. [15], in the course of our exploration of the boron-rich region of the U-Mo-B isotherm at 900 °C [19], we observed and studied a new compound UMo_3B_7, for which we present herein the crystal structure obtained from X-ray single crystal diffraction data and results of low temperature heat capacity, magnetic susceptibility and electrical resistivity studies.

2. Experimental details

Several samples within the 8U:30Mo:62B - 11U:22Mo:67B composition range and a total amount of about 0.5 g each were prepared by argon arc-melting elemental pieces of uranium (purity >99.9%), molybdenum (99.95%) and crystalline

boron (purity >99.8%). The surface of uranium pieces was deoxidized in diluted nitric acid prior to melting. The samples were re-melted several times without significant weight losses (< 1 wt.%). The alloy buttons were sealed in evacuated quartz tubes and annealed at 900 ºC for two weeks before quenching into cold water. X-ray powder diffraction patterns were collected employing a Philips X'Pert diffractometer with Cu K_α radiation within the 2θ range 10-120 deg. Evaluation with the WINPLOTR [20] and FULLPROF [21] programs indicated the formation of a new compound at the approximate composition 9U:27Mo:64B.

YMo_3B_7 (~ 1 g) was prepared from pieces of pure elements (Y 99.9%, Mo 99.95% and B >99.8%) following the above-described procedure. X-ray powder diffraction data were collected employing a Guinier-Huber Image Plate system with monochromatic Cu $K\alpha_1$ radiation (8º<2θ<100º).

Several crystals were mechanically isolated from the crushed $U_{11}Mo_{22}B_{67}$ nominal composition alloy and their crystal structure was investigated with the help of a Bruker AXS SMART CCD diffractometer. Inspection of the first 20 frames of single crystal diffraction data assured high crystal quality, unit cell dimensions and orthorhombic Laue symmetry of the specimens prior to the X-ray intensity data collections. The data set for the best crystal was recorded at room temperature in the ω-scan mode. A total of 2464 frames were collected with a $\Delta\phi$ of 0.3° and an exposure time of 30 s. Data reduction was carried out using the SAINT suite of programs; the intensities were corrected for absorption with the assistance of the program SADABS [22]. Further details of data collection are provided in Table 1. Structure solution and refinement were performed with SHELXS-97 and SHELXL-97 from the WinGX-1.70.00 integrated systems of programs [23, 24].

Physical properties have been studied for the two isostructural compounds, UMo_3B_7 and YMo_3B_7. A superconducting quantum interference device (SQUID) served for magnetization measurements in the temperature interval from 3 to 300 K using bar-shaped polycrystalline specimens of about 20 mg. Specific heat measurements on samples of about the same weight were performed at temperatures ranging from 2 K up to 20 K by means of the conventional relaxation time method in a Quantum Design PPMS. The electrical resistivity of bar shaped samples (about 1x1x5 mm^3) was measured using a four-probe a.c.-bridge method in the temperature range from 0.4 K to room temperature and in fields up to 12 T [25].

3. Crystal structure determination and analysis

Single crystal X-ray intensity pattern indicated a primitive orthorhombic lattice, Laue class *mmm* and systematic extinctions consistent with space group *Pnma* (no. 62). Initial atomic positions for one uranium atom and three molybdenum atoms were found by direct methods, whereas seven boron atoms were located from difference Fourier synthesis. The refinement of the structure proceeded straight-forwardly adopting anisotropic temperature factors for the metal atoms but isotropic thermal displacement parameters for boron atoms (Table 1) and led to a residual value as low as R_F^2=0.0205. Standardization of the atomic positions with program Structure Tidy [26] confirmed isotypism with the structure model of YMo_3B_7 [27]. Good agreement with the parent structure was also observed for the values of interatomic distances (d_{U-U}=0.30995(2) nm and d_{Y-Y}=0.3101 nm; B-B distances range from 0.1759(9) nm for B1-B4 to 0.1843(9) nm for B3-B6, etc.) (Table 2). The coordination numbers of metal atoms were found to be 22 for uranium and 15, 17 and 20 for Mo1, Mo2 and Mo3 respectively: [$UB_{12}Mo_8U_2$], [$Mo1B_9Mo_4U_4$], [$Mo2B_9Mo_5U_3$] and [$Mo3B_{12}Mo_7U$]. A three dimensional view of the UMo_3B_7 structure is shown in Figure 1. Boron atoms are bonded to form slightly puckered bands composed of six rows of edge-linked hexagons extended infinitely in the *b* direction and tilted to the *ab*-plane. All boron atoms are placed in triangular prisms formed by metal atoms with three (for B1, B2, B3, B4, B5 and B6) or two (for B7) additional atoms of boron located against triangular faces. In UMo_3B_7, the trigonal [BM_6] prisms (M=U, Mo) share triangular (and rectangular) faces to form slabs running infinitely along the *b* axis. In the *ac*-plane, the slabs are separated by infinite columns of unfilled tetrahedra [Mo_2U_2] and tetragonal pyramids [Mo_4U]. These three structural units also constitute the structure of CrB [28] (Figure 2c), which is composed, in terms of structural fragments, of W-type slabs (infinite planar layers of face-linked unfilled tetrahedra and tetragonal pyramids formed by Cr atoms) inter-leaving with AlB_2-type slabs (B-filled trigonal prisms [BCr_6] (Figure 2b) as well as they form the structures of related monoborides FeB, α-MoB and their ternary derivative $NbCoB_2$. Boron atoms in these structures form infinite zigzag boron chains. In numerous structures with metal/boron ratios larger than 1.5, two or three B zigzag chains are connected at bonding distances thus forming double or triple chains [9]. This tendency toward two-dimensional net

formation (e.g. AlB_2-type) with increasing boron content is recognized from the structural series within the V-B system: V_nB_{n+1}=(n-1)VB (CrB-type) + VB_2 (AlB_2-type) (n=1,2,3,5) [29]. In V_2B_3 (Figure 2d), three B zigzag chains are connected to form planar bands of B_6 hexagons extending infinitively along the *c* axis; correspondingly the structure is composed of slabs of three layers of close packed [BV_6] trigonal prisms. Two slabs are inter-linked via unfilled rectangular pyramids and tetrahedra formed by vanadium atoms. In UMo_3B_7, the slabs are composed of 7 layers of slightly distorted [BM_6] trigonal prisms and terminate with the columns of rectangular pyramids and tetrahedra (Figure 2a). Contrary to the V_2B_3 structure, the slabs are shifted with respect to each other along the *x*-axis; each column is linked via U-Mo bonds with another column, which in turn gives rise for a new slab built of 7 layers of [BM_6] trigonal prisms. Condensation of prisms in the *ac* plane is realized by metal-metal bonds in such a way that every consequent corrugated layer is composed of only trigonal prisms connected by triangular-faces, while the remaining layers resemble the arrangement of fragments in the transposition structure of CrB, the FeB [30] and exhibit the rectangular pyramids and tetrahedra interleaved with one or two [BM_6] trigonal prisms.

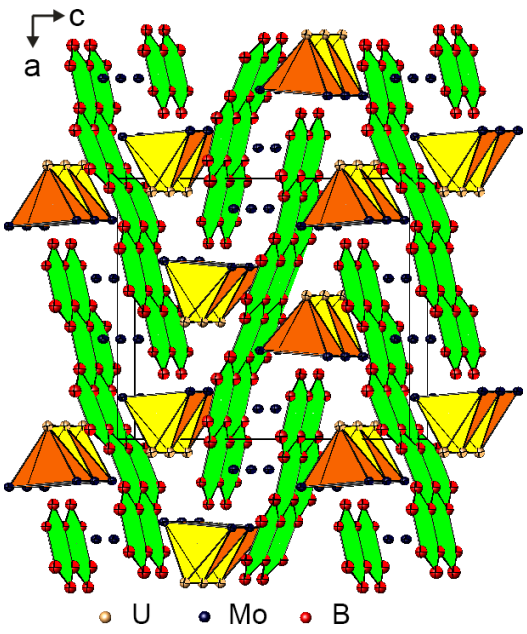

Fig. 1. Unit cell of UMo_3B_7 emphasizing structural fragments: boron sub-lattice, and columns of unfilled tetragonal pyramids and tetrahedra formed by metal atoms. Bonds interlinking those fragments are omitted for clarity.

Table 1

Crystal structure data[a] for UMo_3B_7 and YMo_3B_7 (YMo_3B_7-type structure, space group *Pnma* (no. 62), Z=4)

Nominal composition	$U_{9.09}Mo_{27.27}B_{63.64}$	$Y_{9.09}Mo_{27.27}B_{63.64}$
Formula from refinement	UMo_3B_7	YMo_3B_7
Diffractometer	Bruker AXS SMART CCD, MoK_α	Guinier-Huber Image Plate, $CuK_{\alpha1}$
Theta range	$7.40°<2\theta<69.96°$	$10°<2\theta<100°$
Crystal size	$20x20x40\mu m^3$	-
a [nm]	1.10310(8)	1.10136(2)
b [nm]	0.30995(2)	0.310244(5)
c [nm]	1.2792(1)	1.28597(2)
Reflections in refinement	1040 Fo $>4\sigma$ (Fo) of 1092	159
Mosaicity	<0.4	-
Number of variables	47	42
Reliability factors	$R_F^2=\Sigma\lvert F_o^2-F_c^2\rvert/\Sigma F_o^2=0.0205$ wR2=0.0553 GOF=1.021 -	$R_F=\Sigma\lvert F_o-F_c\rvert/\Sigma F_o=0.049$ $R_I=\Sigma\lvert I_o-I_c\rvert/\Sigma I_o=0.073$ $R_{exp}=[(N-P+C)/\Sigma w_i y^2_{oi})]^{1/2}=0.018$ $\chi^2=(R_{wP}/R_e)^2=8.50$
Extinction (Zachariasen)	0.0034(2)	-
M1[b]; Occ.;	*x*=0.44931(2), *z*=0.69300(2); 1.00 U1;	*x*=0.4501(2), *z*=0.6920(2); 1.00 Y1;
U_{11}[c,d]; U_{22}; U_{33};	0.0040(1); 0.0049(1); 0.0044(1)	-
B_{iso}[c]	-	0.44(8)
Mo1; Occ.;	*x*=0.31665(4), *z*=0.20508(2); 1.00;	*x*=0.3130(2), *z*=0.2028(2); 1.00;
U_{11}; U_{22}; U_{33};	0.0030(2); 0.0044(2); 0.0042(2)	-
B_{iso}	-	0.42(8)
Mo2; Occ.;	*x*=0.33957(4), *z*=0.43667(4); 1.00;	*x*=0.3389(2), *z*=0.4361(2); 1.00;
U_{11}; U_{22}; U_{33};	0.0028(2); 0.0048(2); 0.0037(2)	-
B_{iso}	-	0.58(9)
Mo3; Occ.;	*x*=0.88360(4), *z*=0.52688(4); 1.00;	*x*=0.8823(2), *z*=0.5277(2); 1.00;
U_{11}; U_{22}; U_{33};	0.0032(2); 0.0054(2); 0.0046(2)	-
B_{iso}	-	0.74(8)
B1; Occ.;	*x*=0.0101(6), *z*=0.3635(5); 1.00;	*x*=0.011(3), *z*=0.362(2); 1.00;
U_{iso}, B_{iso}	0.0066(9)	0.5[e]
B2; Occ.;	*x*=0.0364(6), *z*=0.0177(5); 1.00;	*x*=0.039(3), *z*=0.018(2); 1.00;
U_{iso}, B_{iso}	0.0056(9)	0.5[e]
B3; Occ.;	*x*=0.0685(6), *z*=0.6154(5); 1.00;	*x*=0.069(2), *z*=0.617(2); 1.00;
U_{iso}, B_{iso}	0.0054(9)	0.5[e]
B4; Occ.;	*x*=0.1653(6), *z*=0.3321(5); 1.00;	*x*=0.166(2), *z*=0.333(2); 1.00;
U_{iso}, B_{iso}	0.0044(9)	0.5[e]
B5; Occ.;	*x*=0.1849(6), *z*=0.0685(5); 1.00;	*x*=0.187(2), *z*=0.067(2); 1.00;
U_{iso}, B_{iso}	0.0064(9)	0.5[e]
B6; Occ.;	*x*=0.2316(6), *z*=0.5840(5); 1.00;	*x*=0.230(2), *z*=0.582(2); 1.00;
U_{iso}, B_{iso}	0.0059(9)	0.5[e]
B7; Occ.;	*x*=0.2507(6), *z*=0.8262(5); 1.00;	*x*=0.248(2), *z*=0.826(3); 1.00;
U_{iso}, B_{iso}	0.0072(10)	0.5[e]
Residual density, max; min [el./nm^3]$x10^3$	2.85; -2.19	-

[a] Crystal structure data are standardized using the program Structure Tidy[25]; [b] All atoms in *4c* (*x*, ¼, *z*); [c] Anisotropic U_{ij} (isotropic U_{iso}, B_{iso}) atom displacement parameters are given in $Å^2$; [d] $U_{13}=U_{23}=U_{12}=0$; [e] Fixed parameter

Table 2

Selected interatomic distances (×10 nm) for UMo_3B_7

U1-2B5	2.670(5)	Mo2 - B6	2.230(6)	B1- B4	1.759(9)	B4- B1	1.759(9)
-2B4	2.678(5)	- B2	2.230(6)	-2B3	1.796(5)	-2B7	1.807(4)
-2B1	2.713(5)	-2B5	2.307(5)	- Mo1	2.307(7)	- Mo1	2.330(6)
-2B2	2.729(5)	-2B2	2.313(5)	-2Mo3	2.397(5)	- Mo2	2.340(6)
- B7	2.776(6)	-2B7	2.322(5)	- Mo3	2.513(6)	-2Mo3	2.438(5)
- B6	2.777(6)	- B4	2.340(6)	-2U1	2.713(5)	-2U	2.678(5)
- B3	2.781(6)	-2Mo3	2.9461(6)				
- B2	2.863(6)	- Mo1	2.9733(8)	B2- B5	1.762(9)	B5- B2	1.762(9)
-2U1	3.0995(2)	-2Mo2	3.0995(2)	-2B2	1.805(5)	- 2B6	1.813(5)
-2Mo2	3.2522(5)	-2U1	3.2522(5)	- Mo2	2.249(7)	- Mo1	2.271(7)
-2Mo1	3.2813(5)	- U1	3.4953(6)	-2Mo2	2.313(5)	- 2Mo2	2.307(5)
-2Mo1	3.3216(5)			-2U1	2.729(5)	- Mo3	2.508(7)
- Mo2	3.4953(6)	Mo3- B3	2.333(7)	- U1	2.863(6)	- 2U1	2.670(5)
- Mo3	3.6568(5)	- B7	2.384(6)				
		-2B1	2.397(5)	B3-2B1	1.796(5)	B6-2B5	1.813(5)
Mo1-2B6	2.255(5)	-2B4	2.438(5)	- B6	1.843(9)	- B3	1.843(9)
- B5	2.271(7)	-2B3	2.448(5)	-2Mo1	2.307(5)	- Mo2	2.230(6)
-2B3	2.307(5)	-2B6	2.455(5)	- Mo3	2.333(7)	- 2Mo1	2.255(5)
- B1	2.307(7)	- B5	2.508(7)	-2Mo3	2.448(5)	- 2Mo3	2.455(5)
-2B7	2.314(5)	- B1	2.513(6)	- U1	2.781(6)	- U1	2.777(7)
- B4	2.330(6)	-2Mo2	2.9461(6)				
- Mo2	2.9733(8)	- Mo1	3.0578(8)			B7-2B4	1.807(4)
- Mo3	3.0578(8)	-2Mo3	3.0772(6)			-2Mo1	2.314(5)
-2Mo1	3.0995(2)	-2Mo3	3.0995(2)			-2Mo2	2.322(5)
-2U1	3.2813(5)	- U1	3.6568(5)			- Mo3	2.384(7)
-2U1	3.3216(5)					- U1	2.776(7)

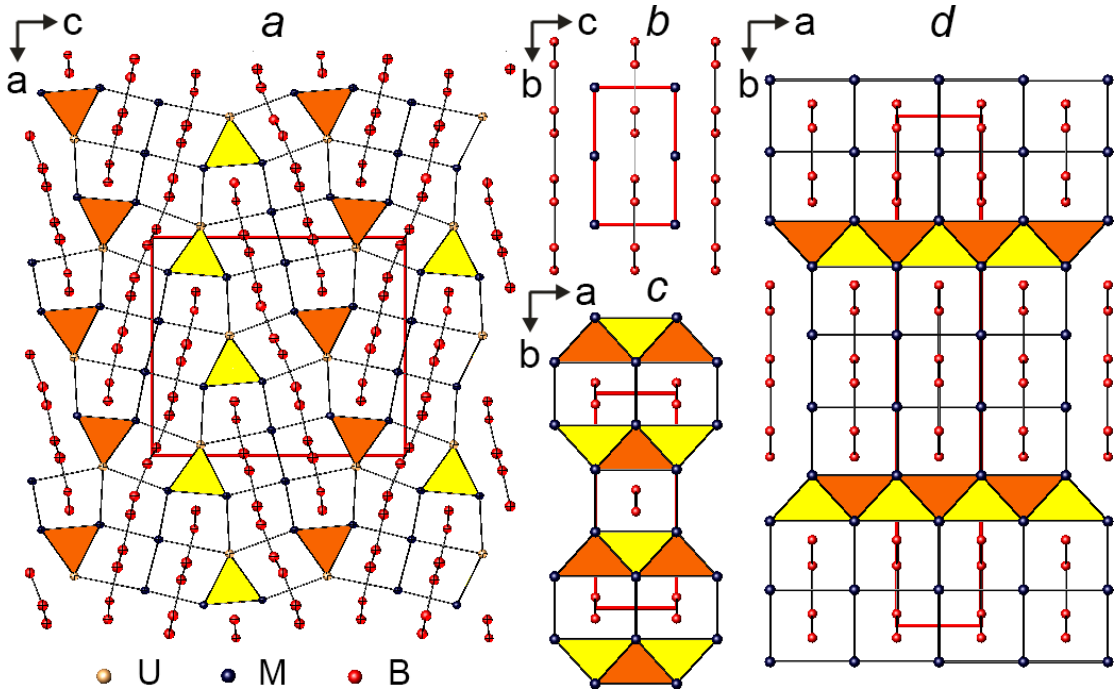

Fig. 2. UMo_3B_7 structure (a) in comparison with AlB_2 in orthorhombic setting (b), CrB (c) and V_2B_3 (d). M stays for Al, Cr, V and Mo.

4. Physical properties

Figure 3 shows the temperature dependence of the electrical resistivity of UMo_3B_7 together with the resistivity of non magnetic YMo_3B_7. The resistivity of the latter behaves as expected for simple metals, and can be described in terms of the Bloch-Grüneisen model:

$$\rho_{ideal} = \rho_0 + C\frac{T^5}{\theta_R{}^6}\int_0^{\theta_R/T}\frac{x^5}{(e^x-1)(1-e^{-x})}dx \qquad (1)$$

where ρ_0 is the residual resistivity due to charge carrier scattering on static lattice defects and the second term represents the scattering of electrons on thermally excited phonons. Such an approach gives a Debye temperature, $\theta_R = 341\text{K}$ and a residual resistivity value $\rho_0 = 9.5\,\mu\Omega\text{cm}$ as a result of a least squares fitting (solid line, Fig.3).

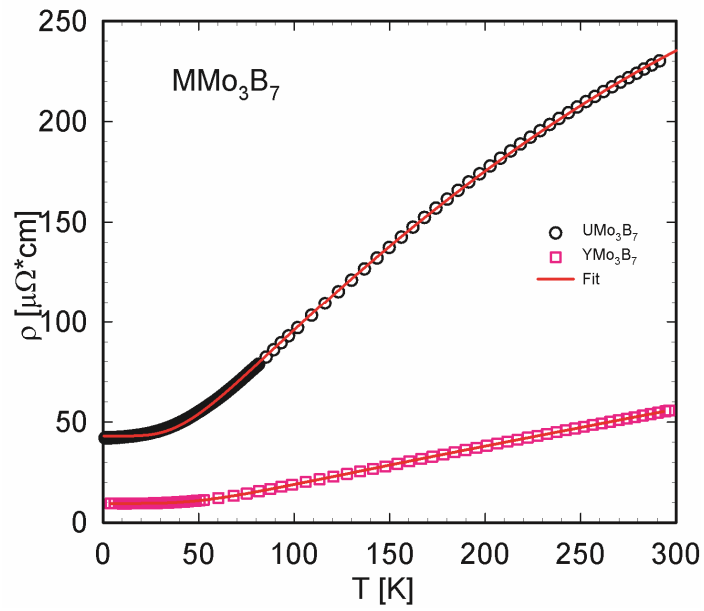

Fig. 3. Temperature dependent electrical resistivity of UMo_3B_7 and nonmagnetic YMo_3B_7. Solid line is a least square fit according to the Bloch-Grüneisen relation.

The resistivity of the uranium compound increases with increasing temperature demonstrating a metallic behaviour with no anomalies in the entire temperature range studied. However, in the high temperature region the resistivity of

UMo_3B_7 exhibits a tendency to saturate due to *s-d* interband scattering, and thus the Bloch-Grüneisen-Mott formula

$$\rho_{B-G-M} = \rho_0 + C\frac{T^5}{\theta_R{}^6}\int_0^{\theta_R/T}\frac{x^5}{(e^x-1)(1-e^{-x})}dx - AT^3 \qquad (2)$$

is taken into account, delivering $\rho_0 = 43\ \mu\Omega\text{cm}$, $\theta_R = 267\ K$ and a Mott coefficient, $A = 1.2*10^{-6}\ \mu\Omega/cmK^3$. Despite the good agreement of the Bloch-Grüneisen-Mott formula with the experimental data in the high temperature region, in the low temperature range the resistivity of UMo_3B_7 is no longer dominated by phonons, but rather changes towards a T^2 behaviour. A similar behaviour of the resistivity is also observed in applied magnetic fields (see Figure 4b), where the $\rho(T)$ *vs* T^2 curves are strictly linear for all magnetic fields in the temperature region below 10 K.

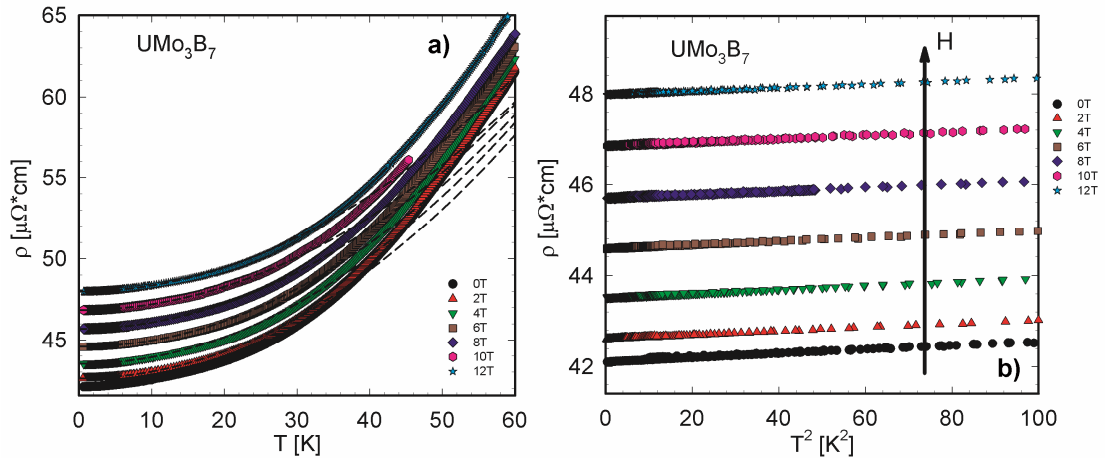

Fig. 4. a) Temperature dependent electrical resistivity of UMo_3B_7 measured at various external magnetic fields up to 12 T. The dashed lines correspond to $\rho(T)=\rho_0+A_HT^2$ fits. b) Resistivity as a function of T^2 for temperatures below 10 K.

The magnetoresistance of UMo_3B_7 is presented on Fig. 5a in a form of $\frac{\rho(H,T)-\rho(0,T)}{\rho(0,T)}$. It is positive at all the temperatures studied (from 0.5 to 50 K), monotonously increases with increasing fields and decreases as the temperature raises. Such a behaviour is a typical feature of the so called classical magnetoresistance, where the increase in resistivity with the magnetic field is understood in terms of the magnetic field driven orbital motion of conduction

electrons. This influence should produce a $\Delta\rho_{nmr}(H,T) = A(T)H^2$ behaviour, where $A(T)$ decreases with increasing temperature. However this is not the case for the magnetoresistance of UMo_3B_7, where $\frac{\rho(H,T)-\rho(0,T)}{\rho(0,T)}$ was found not to be dependent on H^2, but rather follows a weaker power law, hinting to magnetic interactions producing a negative contribution to the total magnetoresistance. Moreover, the Kohler's rule is not well satisfied (see inset Fig 5a). Such a behaviour is typically found in spin fluctuating systems.

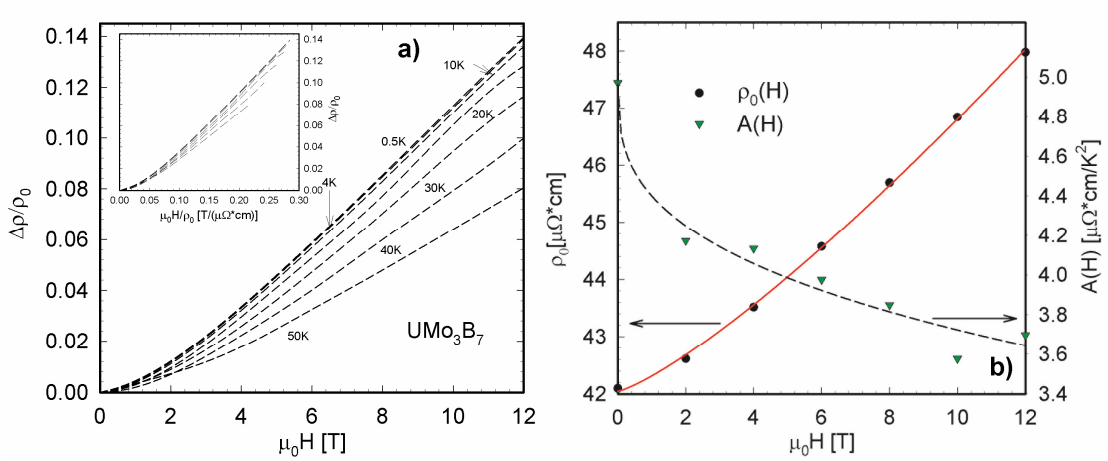

Fig. 5. a) Field dependent magnetoresistance of UMo_3B_7 at various temperatures. The inset shows the Kohler's graph for the same compound. b) Residual resistivity ρ_0 of UMo_3B_7 together with the temperature independent coefficient A(H) as a function of external magnetic fields. The solid line corresponds to the fit described in the text. The dashed line is drawn as a guidance for the eye.

For temperatures below 5 K, the behaviour of the electrical resistivity of UMo_3B_7 as a function of magnetic field and temperature is well described by

$$\rho(H,T) = \rho_0(H) + A(H)T^2 . \qquad (3)$$

Fig. 5b displays the field-dependence of ρ_0 (left axis). The residual resistivity monotonously increase with increasing fields, $\rho_0 \propto T^{1.25}$ (see Fig 5b). A(H) decreases with increasing field, taking a rapid drop at low fields but does not show the tendency to saturate in fields up to 12T. Such a behaviour is common in many spin fluctuating systems, see for example Ref. [31].

The temperature dependent magnetic susceptibility of UMo_3B_7 is presented in Figure 6a. The compound exhibits a moderately enhanced (of the order of 10^{-3} emu/mol) and almost temperature independent susceptibility, showing no signs of magnetic transitions in the entire temperature range. In the temperature region above 100 K the data were analyzed using the modified Curie-Weiss law,

$$\chi = \frac{C}{T - \theta_p} + \chi_0 , \tag{4}$$

delivering the paramagnetic Curie temperature $\theta_p = -45$ K and a temperature independent magnetic susceptibility $\chi_0 = 1.27 * 10^{-3}$ emu/mol. In the temperature region below 50 K, however, the experimental values of the magnetic susceptibility are lower than those expected from the Curie-Weiss behavior. Subtracting the first term of Eqn. 4 from the approximated experimental data, $\chi_0^*(T)$ is found to increase with temperature, reaching $\chi_0 = 1.27 * 10^{-3}$ emu/mol at around 70 K.

Fig. 6b represents the low temperature dependence of the specific heat C_p of UMo_3B_7, plotted as $C_p(T)/T$ versus T^2. Down to 2 K no evidence of any magnetic ordering was observed, in agreement with resistivity and magnetic susceptibility data. On the other hand, a simple metallic behavior of specific heat, i.e., $C_p = \gamma T + \beta T^3$ is found only for a limited temperature range above 10 K. In the low temperature region the behavior of the specific heat of UMo_3B_7 can be much better approximated by a spin fluctuation model, i.e.,

$$C_p(T) = \gamma T + AT^3 + BT^3 \ln \frac{T}{T^*} , \tag{4}$$

revealing an enlarged Sommerfeld coefficient $\gamma = 28\,\mathrm{mJ/(molK^2)}$ and a characteristic temperature $T^* = 6$ K. This suspects spin fluctuations in a nearly localized regime.

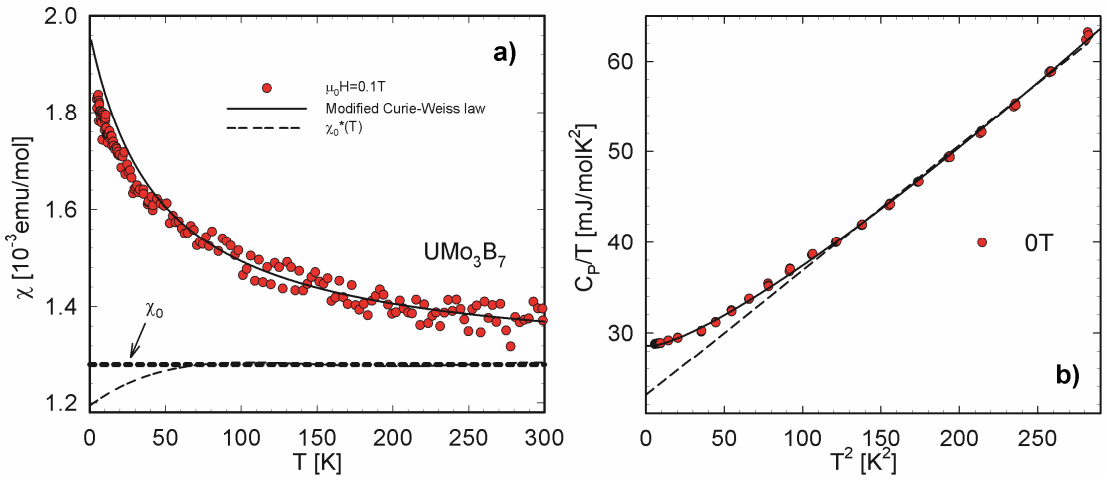

Fig. 6. a) Temperature dependent magnetic susceptibility of polycrystalline UMo_3B_7 measured in a field of 0.1 T. The solid line corresponds to the high temperature modified Curie-Weiss fit as described in the text. The dashed line describes the temperature dependence of $\chi_0^*(T)$. b) Low-temperature specific heat C_P plotted as $C_p(T)/T$ vs T^2. The solid line is a least-squares fit according to Eqn. 4. The dashed line corresponds to a behaviour according to $C_p = \gamma T + \beta T^3$.

5. Summary

A new ternary compound, UMo_3B_7, was identified in the U-Mo-B system at 900 °C. The crystal structure was studied by single crystal X-ray diffraction: YMo_3B_7 type, space group Pnma, a=1.10310(8) nm, b=0.30995(2) nm, c=1.2792(1). From the relation between the metal:boron ratio [9] and the type of boron atoms linkage established for other boride structures (Er_3CrB_7 [32], $La_2Re_3B_7$ [33, 34], $W_2Ir_3B_5$ [35], etc) where the boron atoms form folded infinite chains, the formation of higher boron aggregates in UMo_3B_7 (metal:boron ratio 0.57) is expected. Accordingly, in the UMo_3B_7 the -B- chains (formed by -B1-B4- at d=0.1759 nm, -B3-B6- at d=0.1843 nm, and -B2-B5- at d=0.1762 nm) come close together (d_{B1-B3}=0.1796 nm, d_{B2-B2}=0.1805 nm, d_{B4-B7}=0.1807 nm, d_{B5-B6}=0.1813 nm) to build 6^3 boron bands. Considering the metal atoms framework, UMo_3B_7 has common fragments with the structure of CrB: B-filled trigonal prisms, and unfilled tetrahedra and tetragonal pyramids.

UMo_3B_7 does not exhibits long range magnetic order above 500mK. Rather a spin fluctuation scenario characterizes the low temperature behavior of resistivity,

magnetic susceptibility and specific heat of this compound, resulting in a moderately enlarged Sommerfeld value $\gamma = 28\,\mathrm{mJ/(molK^2)}$.

ACKNOWLEGMENTS. Research supported by Austrian National Science Foundation FWF V279-N19. L.S. is thankful to OÄD for a fellowship. This work was partially supported in Portugal with funds from FEDER (Programa Operacional Factores de Competividade COMPETE-2020) and from FCT - Fundação para a Ciência e Tecnologia under projects Nb 016789 PTDC/FIS-NAN/6099/2014 and UID/Multi/04349/2013.

References

[1] S. Souma, Y. Machida, T. Sato, T. Takahashi, H. Matsui, S.C. Wang, H. Ding, A. Kaminski, J.C. Campuzano, S. Sasaki, K. Kadowaki, The origin of multiple superconducting gaps in MgB_2, Nature 423 (2003) 65-65.

[2] J. Nagamatsu, N. Nakagawa, T. Muranaka, Y. Zenitani, J. Akimitsu, Superconductivity at 39 K in magnesium diboride, Nature 410 (2001) 63-64.

[3] S. Nakatsuji, K. Kuga, Y. Machida, T. Tayama, T. Sakakibara, Y. Karaki, H. Ishimoto, S. Yonezawa, Y. Maeno, E. Pearson, G.G. Lonzarich, L. Balicas, H. Lee, Z. Fisk, Superconductivity and quantum criticality in the heavy-fermion system β-$YbAlB_4$, Nature Physics 4 (2008) 603-607.

[4] R.T. Macaluso, S. Nakatsuji, K. Kuga, E.L. Thomas, Y. Machida, Y. Maeno, Z. Fisk, J.Y. Chan, Chem. Mater. Crystal structure and physical properties of polymorphs of $LnAlB_4$ (Ln = Yb, Lu) 19 (2007) 1918-1922.

[5] Y. Matsumoto, S. Nakatsuji, K. Kuga, Y. Karaki, N. Horie, Y. Shimura, T. Sakakibara, A.H. Nevidomskyy, P. Coleman, Quantum criticality without tuning in the mixed valence compound β-$YbAlB_4$, Science 331 (2011) 316-319.

[6] K. Yubuta, T. Mori, S. Okada, Yu. Prots, H. Borrmann, Yu. Grin, T. Shishido High-resolution electron microscopy and X-ray diffraction study of intergrowth structures in α- and β-type $YbAlB_4$ single crystals, Philosophical Magazine, 93 (2013) 1054-1064.

[7] D.A. Tompsett, Z.P Yin, G.G. Lonzarich, W.E. Pickett, Role of crystal symmetry in the magnetic instabilities of β-$YbAlB_4$ and α-$YbAlB_4$, Phys. Rev. B 82 (2010) 235101.

[8] Yu.B. Kuz'ma, S.I. Svarichevskaya, Crystal structure of compounds Y_2ReB_6 and their analogous, J. Sov. Phys. Crystallogr. 17 (1972) 569-571.

[9] P. Rogl, Existence and Crystal Chemistry of Borides, in: J.J. Zuckerman (Ed.), Inorganic Reactions and Methods, VCH-Publications Inc., 1991, 13(6), 85-167 and references therein.

[10] A.M. Alekseeva, A.M. Abakumov, P.S. Chizhov, A. Leithe-Jasper, W. Schnelle, Yu. Prots, J. Hadermann, E.V. Antipov, Yu. Grin, Ternary magnesium rhodium boride $Mg_2Rh_{1-x}B_{6+2x}$ with a modified Y_2ReB_6-type crystal structure, Inorg. Chem. 46 (2007) 7378-7386.

[11] A.M. Alekseeva, Yu. Prots, A. Leithe-Jasper, E.V. Antipov, Yu. Grin, Crystal structure of magnesium iridium boride, $Mg_2Ir_{1-x}B_{6+2x}$ (x=0.3), Z. f Kristallogr. - New Crystal Structures 224 (2009) 19-20.

[12] T. Mori, T. Shishido, K. Yubuta, K. Nakajima, A. Leithe-Jasper, Yu. Grin, Physical properties of β-$TmAlB_4$ an AlB_2-type analogous ``tiling'' compound, J. Appl. Phys. 107 (2010) 09E112-3.

[13] T. Mori, S. Okada, K. Kudou, Magnetic properties of thulium aluminoboride $TmAlB_4$, J. Appl. Phys. 97 (2005) 10A910-3.

[14] T. Mori, H. Borrmann, S. Okada, K. Kudou, A. Leithe-Jasper, U. Burkhardt, Yu. Grin, Crystal structure, chemical bonding, electrical transport, and magnetic behavior of $TmAlB_4$, Phys. Rev. B 76 (2007) 064404.

[15] I.P. Valyovka, Yu.B. Kuzma, Isothermal section of the diagram of the systems U-Mo-B and U-Re-B, Sov. Powder Metall. Met. Ceram. 25 (1986) 986-988.

[16] P. Rogl, H. Nowotny, Complex borides with uranium, Monatsh. Chem. 106 (1975) 381-387.

[17] P. Rogl, L. DeLong, New ternary transition metal borides containing uranium and rare earth elements, J. Less-Common Met. 91 (1983) 97-106.

[18] T. Konrad, W. Jeitschko, $U_5Mo_{10}B_{24}$, a boride containing three different kinds of boron polyanions, J. Alloys Comp. 233 (1996) L3-L7.

[19] L Salamakha, C Rizzoli, S Mudryi, M Almeida, U–Mo–B System: Phase Equilibria at 900ºC and Crystal Structure of Compounds**,** 43èmes Journées des Actinides, 6-9 April 2013, Sestri Levante, Italy

[20] T. Roisnel, J. Rodriguez-Carvajal, 2000 WinPLOTR: a Windows tool for powder diffraction patterns analysis, in: R. Delhez, E.J. Mittenmeijer (Eds.) Materials Science Forum, Proceedings EPDIC 7 (2000) 118-123.

[21] J. Rodriguez-Carvajal, Recent advances in magnetic structure determination by neutron powder diffraction, Physica B 192 (1993) 55-69.

[22] SMART, SAINT, and SADABS Packages. Version 5.1. Bruker AXS. Madison WI 1997–1999.

[23] G.M. Sheldrick, A short history of *SHELX,* Acta Cryst. A64 (2008) 112-122.

[24] L.J. Farrugia, *WinGX* suite for small-molecule single-crystal crystallography, J. Appl. Cryst. 32 (1999) 837-838.

[25] E. Bauer, St. Berger, Ch. Paul, M. Della Mea, G. Hilscher, H. Michor, M. Reissner, W. Steiner, A. Grytsiv, P. Rogl, E.-W. Scheidt, Crystal field effects and thermoelectric properties of $PrFe_4Sb_{12}$ skutterudite, Phys Rev B 66 (2002) 214421.

[26] E. Parthé, L. Gelato, B. Chabot, M. Penzo, K. Censual, R. Gladyshevskii, TYPIX –Standardized Data and Crystal Chemical Characterization of Inorganic Structure Types, Gmelin Handbook of Inorganic and Organometallic Chemistry, 8th edition (1994).

[27] S.I. Mikhalenko, V.S. Babizhetskii, H. Hartl, Yu.B. Kuzma, New YMo_3B_7 boride and its structure, Crystallogr. Rep. 40 (1995) 424-427.

[28] R. Keissling, The binary system chromium - boron, Acta Chem Scand 3 (1949) 595-602.

[29] K.E. Spear, P.W. Gilles, Phase and structure relationships in the vanadium-boron system, High Temp. Sci. 1 (1969) 86-97.

[30] D. Hohnke, E. Parthé, *AB* compounds with Sc,Y and rare earth metals. II. FeB and CrB structures of monosilicides and germanides, Acta Cryst. 20 (1966) 572-582.

[31] K. Ikeda, K.A. Gschneidner Jr., N. Kobayashi, K. Noto, Magnetoresistance of Sc_3In, J. Magn. Magn. Mater. 42 (1984) 1-11.

[32] N.F. Chaban, L.G. Aksel'rud, V.A. Bruskov, Yu.B Kuz'ma, Crystal structure of the new boride Er_3CrB_7, Sov. Phys. Crystallogr. 30 (1985) 108-109.

[33] Yu.B. Kuzma, S.I. Mykhalenko, B.Ya. Kotur, Ya.P. Yarmolyuk, The crystal structure of boride $La_2Re_3B_7$, Dopov. Akad. Nauk Ukr. RSR B 3 (1982) 24-27.

[34] D.E. Bugaris, Ch.D. Malliakas, D.Y. Chung, M.G. Kanatzidis, Metallic Borides, $La_2Re_3B_7$ and $La_3Re_2B_5$, Featuring extensive boron− boron bonding, Inorg. Chem. 55 (2016) 1664−1673.

[35] P. Rogl, F. Benesovsky, H. Nowotny, Complex borides with platinum metals, Monatsh Chem 103 (1972) 965-989.